Understanding catalyst structure-selectivity relationships in Pd-catalyzed enantioselective methoxycarbonylation of styrene

Simone Gallarati,[†,‡] Paul Dingwall,[§] José A. Fuentes,[†] Michael Bühl,[*,†] and Matthew L. Clarke[*,†]

[†]School of Chemistry, University of St Andrews, North Haugh, St Andrews KY16 9ST, UK

[§]School of Chemistry and Chemical Engineering, Queen's University Belfast, Belfast BT9 5AG, UK

ABSTRACT: Catalyst-controlled regioselectivity in palladium-catalyzed carbonylation of alkenes has been a long-standing goal of homogeneous catalysis. In general, monophosphines do favor branched regioselectivity, but lead to poor enantioselectivity, while diphosphines give mainly linear products. Previously, we reported the simultaneous control of regio- and enantioselectivity in the hydroxy- and methoxycarbonylation of vinyl arenes with Pd complexes of the Phanephos ligand. Herein, we present a density functional theory study (B3PW91-D3 level of theory) of the catalytic cycle, supported by deuterium labeling studies, to understand its mechanism. Alkene coordination to a Pd-hydride species was identified as the origin of asymmetric induction and regioselectivity in both the parent Pd/Xylyl-Phanephos catalyst and electron-deficient analogue, and rationalized according to a quadrant-diagram representation. The mechanism by which the preferentially formed pro-(*S*) Pd-alkene complex can isomerize *via* rotation around the palladium–(C=C) bond was investigated. In the parent system, this process is in competition with the methanolysis step that leads to the ester product, and is responsible for the overall loss of regioselectivity. On the other hand, the introduction of electron-withdrawing substituents on the catalyst framework results in the reduction of the methanolysis barriers, making the isomerization pathway energetically unfavorable and so leading simultaneously to high regiocontrol and good enantiomeric ratios.

INTRODUCTION

Palladium-catalyzed alkoxycarbonylation and hydroxycarbonylation of alkenes are important reactions with a variety of useful applications in homogeneous catalysis.[1] One key application has been the multi-tonne scale production of methyl propionate by methoxycarbonylation of ethene.[2] The importance of this catalytic process, which uses a Pd complex derived from a bidentate ligand with bulky bis-*tert*-butylphosphino substituents, led to significant mechanistic work to understand the underlying mechanism, as well as the development of new catalysts.[3] Subsequently, this type of bidentate 1,2-$(CH_2P^tBu_2)_2C_6H_4$ ligand was also found to be very useful in tandem isomerization-methoxycarbonylation of internal alkenes to give linear products.[4] A related reaction is hydroxycarbonylation using water as a nucleophile;[5] this is perhaps more challenging due to possible issues related to catalyst decomposition or solubility, but in general catalysts give broadly similar performances in both of these reactions, once optimized. For example, tandem isomerization-hydroxycarbonylation promoted by Pd catalysts of bulky bis(*tert*-alkyl)phosphine ligands can also be achieved.[6] The reaction mechanism of such alkoxycarbonylations was a cause of some debate, since it is possible to observe intermediates arising from alkene insertion into a methoxy-carbonyl species (methoxycarbonyl mechanism), but also intermediates arising from the more common alkene insertion into a Pd-hydride (hydride mechanism).[2b, 7] Early computational work favored the hydride mechanism, but did not conclusively rule out the other.[7d] The former mechanism could well be operating in the related co-polymerization of CO and ethene, but the hydride mechanism has convincing evidence in its favor as a general pathway for alkene alkoxycarbonylation.[8]

Scheme 1. (Top) Challenges of Pd-Catalyzed Carbonylation of Olefins with Monodentate and Bidentate Ligands. (Bottom) Enantioselective Methoxycarbonylation of Styrene with Pd/(*S*)-Xylyl- and Pd/(*S*)-F24-Phanephos Catalysts, Showing Pronounced Ligand-Electronic Effect on Regioselectivity.

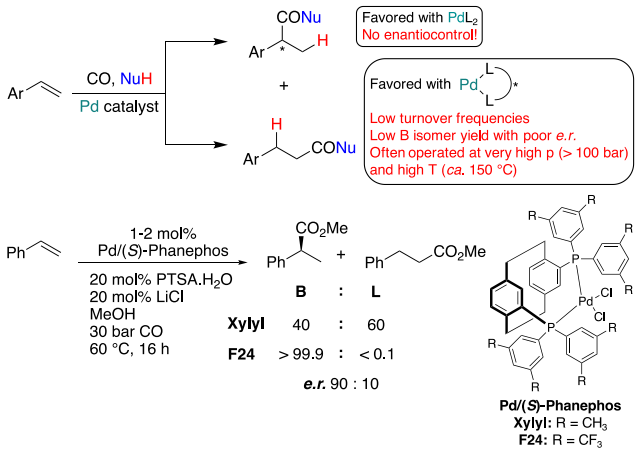

One of the first envisaged applications of alkoxycarbonylation or hydroxycarbonylation was the branched-selective carbonylation of styrene derivatives to give aryl-propanoic acids: for example, of *para*-isobutyl styrene to give Ibuprofen or its esters.[9] Other non-steroidal anti-inflammatory drugs, such as Naproxen, can also be made by branched-selective hydroxycarbonylation of the parent alkene.[10] In some cases, the actual substrate used is either a 1-aryl ethan-1-ol derivative, or the corresponding benzyl chloride derivative. However, such compounds do not readily react with palladium, but do

readily eliminate to give the parent styrene derivative, which is the likely active substrate, and hence these also are likely to proceed *via* the hydride mechanism.[11] The Ibuprofen and Naproxen examples have both been operated at multi-tonne scales over a period of years as one of the main production methods of these commodity drugs. Both processes use Pd catalysts derived from monodentate ligands, and lead to racemic acids (or esters, in the case of methoxycarbonylation), with high branched selectivity. In the case of Ibuprofen, the final product is racemic, but Naproxen and other related aryl propanoic acid drugs, such as Flurbiprofen,[12] are actually resolved and used as a single enantiomer. The carbonylation of styrene derivatives is clearly a significant reaction, and hence for over 40 years efforts have been made to realize it enantioselectively. Unfortunately, most bidentate phosphines of the type generally used in asymmetric catalysis have significant drawbacks (Scheme 1, top). In general, Pd/diphosphine catalysts show both poor activity, requiring very high temperatures that prevent from achieving high enantioselectivity, and tend to give no selectivity for the desired branched acid or ester.[11, 13] Pd catalysts derived from Phanephos ligands[12, 14] were discovered to operate using quite mild conditions and to give good to excellent *e.r.* (enantiomeric ratio) in both hydroxycarbonylation and methoxycarbonylation of several alkenes, including vinyl arenes. Catalysts derived from a Phanephos ligand with 3,4-dimethylphenyl substituents (Xylyl-Phanephos) have been used for several applications in asymmetric synthesis and often incorporated in ligand screening of catalytic processes (see ref. 15 and references therein), although in the case of Pd-catalyzed methoxycarbonylation of styrene they only show, at best, low branched regioselectivity. Building on observations that achiral fluorinated diphosphines lead to better branched regioselectivity,[13a, 16] it was found that F24-Phanephos, the Phanephos ligand with 3,5-bis-trifluoromethylphenyl substituents, enables essentially perfect branched regioselectivity, with quite similar enantioselectivity in the methoxycarbonylation of styrene (Scheme 1, bottom).[14b] Further developments in enantioselective methoxycarbonylation are still desired and are ongoing: for an interesting recent example of enantioselective carbonylation using a CO surrogate, see ref. 17. In general, there is little mechanistic understanding of the Pd/Phanephos carbonylation catalysts, of the reason why bidentate diphosphine ligands often give poor branched regioselectivity, and of the interesting ligand electronic effect that leads to highly regioselective catalysts. This provided the impetus to study this catalytic cycle computationally, and here we show how density functional theory (DFT) computations can provide an understanding of all these issues.

COMPUTATIONAL METHODS

All DFT computations were carried out with the Gaussian 09 software package.[18] Pruned integration grids with 99 radial shells and 590 angular points per shell were used. The hybrid B3PW91 functional[19] was used throughout. In a benchmark study by Bühl and co-workers, this functional was demonstrated to be appropriate for the optimization of several second-row transition metal complexes.[20] Geometry optimizations were undertaken with the 6-31G(d,p) basis set on all non-metal atoms and the SDD (Stuttgart/Dresden ECP)[21] pseudopotential and valence basis for palladium. Dispersion corrections were implemented using Grimme's DFT-D3 correction.[22] In line with our recent study on Rh-catalyzed hydroformylation,[23] in which the neglect of D3 corrections was found to lead to the wrong regioselectivity prediction, dispersion effects were included in the optimization stage as well as single points. Unscaled harmonic frequency calculations at the same level of theory were performed to validate each structure as either a minimum or a transition state and evaluate zero-point corrections. On the basis of the optimized structures, single-point energy refinements were performed with the 6-311+G(d,p) basis set on all non-metal atoms and the SDD effective core potential and valence basis set on palladium. Dispersion corrections were described again with Grimme's DFT-D3 method, while solvent effects in methanol were accounted for using the polarizable continuum model (PCM)[24] approach ($\varepsilon = 32.61$). The single-point electronic energies of species **pro-(*R*)/(*S*)** and **pro-L**, **TS1–2**, $\mathbf{TS_{rotation}}$ and all methanolysis transition states were corrected for intramolecular basis set superposition error using the counterpoise method.[25] Thermochemical corrections at the experimentally relevant temperature of 333.15 K were calculated using the rigid-rotor-harmonic-oscillator approximation with the *GoodVibes* program.[26] According to the scheme proposed by Martin and co-workers (MHP scheme),[27] entropies were evaluated at an elevated pressure to model the translational degrees of freedom in the condensed phase. An empirical correction of $(n - m) \times 3.02$ kcal mol^{-1} (see the Supporting Information for full derivation) was applied to the free energy of a reaction from m-components to n-components in order to model the translational degrees of freedom in the condensed phase and account for different molecularities across distinct parts of the catalytic cycle. All discussed energy differences are based on Gibbs free energies at 333.15 K relative to the reference state (ΔG_{RRS}). Transition states on the potential energy surface were located using scans and a coordinate driving methodology and were confirmed using intrinsic reaction coordinate calculations (IRC).[28] All intermediates were optimized, where possible, from the end point of IRC computations to ensure continuous pathways had been located. Due to the complicated conformational behavior of many intermediates and TSs, considerable care has been taken to identify favored conformers. All structures reported are the most energetically stable ones of those sampled; different conformers of the same stationary point are herein discussed only when relevant to the mechanistic understanding. 3D structures were prepared with CYLview,[29] with C–H bonds hidden for clarity. The SambVca 2.1 web application was used to generate the topographic steric maps.[30]

Scheme 2. Proposed Branched and Linear Catalytic Cycles for Pd-catalyzed Methoxycarbonylation of Styrene with Xylyl- and F24-Phanephos-derived Ligands.

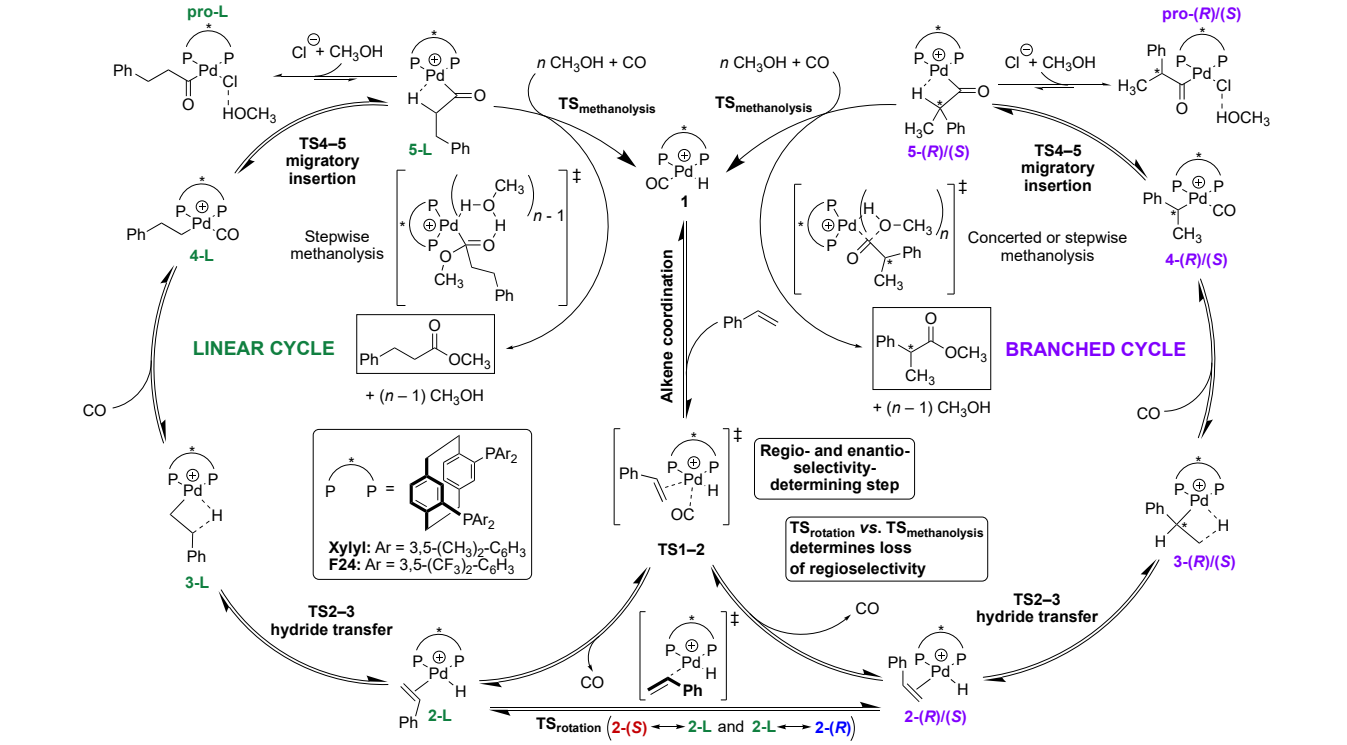

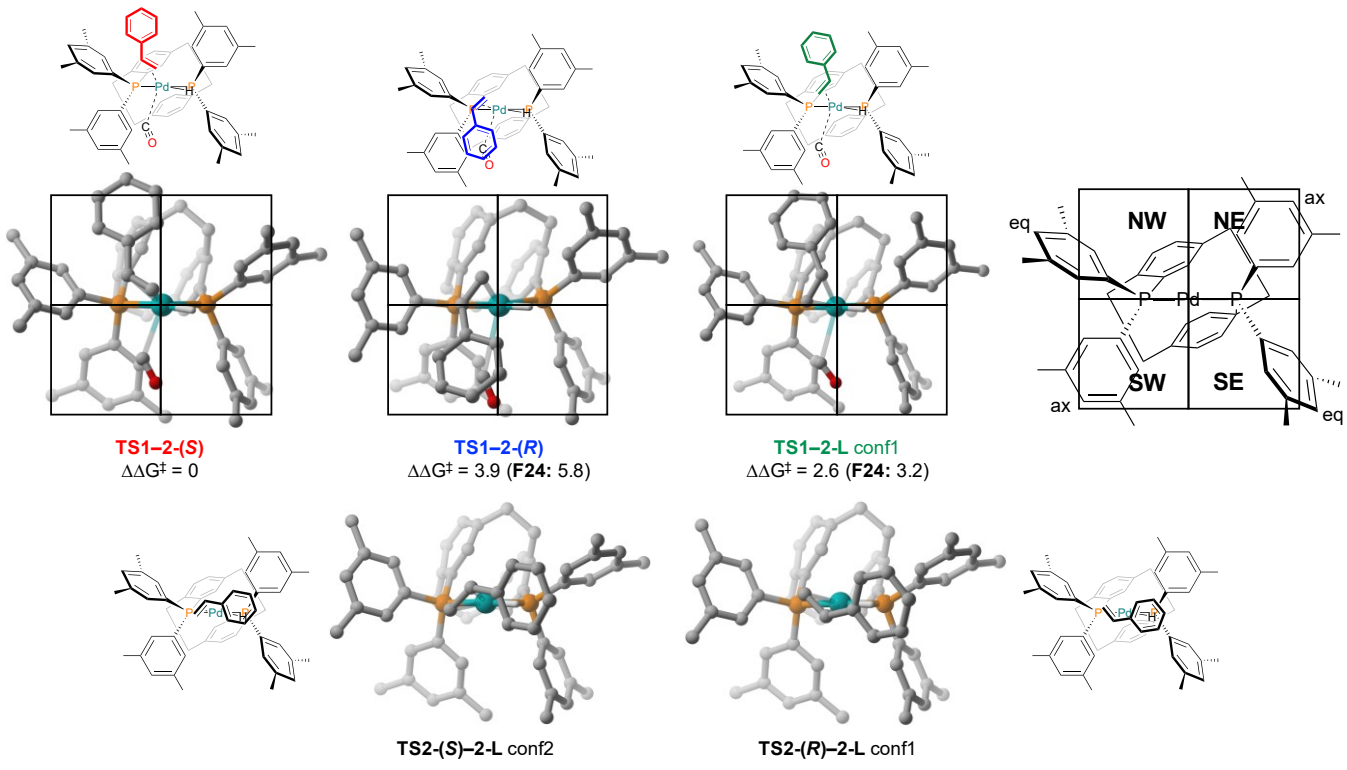

Figure 1. (Top) Optimized geometries and relative free energies of alkene coordination transition state **TS1–2** with the Pd/(*S*)-Xylyl-Phanephos catalyst, showing two-dimensional quadrant representation. Strong steric repulsions are represented in dark red, mild steric hindrance in light red, and the favorable quadrant for coordination in green. Energies are Gibbs free energies in kcal mol^{-1} relative to the (*S*)-TS. (Bottom) Optimized geometries of the rotation transition states connecting the Pd-alkene species.

RESULTS AND DISCUSSION

Catalytic Cycle of Pd/(*S*)-Phanephos–Styrene Methoxycarbonylation. Based on key experimental evidence for the

methoxycarbonylation of ethene,[7c, 31] along with combined experimental and theoretical evidence for the methoxycarbonylation of longer chain alkenes (formed after an isomerization step), it is now accepted that alkoxycarbonylation of alkenes proceeds *via* the hydride mechanism. A variety of different palladium sources can be used in the methoxycarbonylation of alkenes. $Pd^{(0)}$ sources can simply undergo oxidative addition of sulfonic acids to form species of the type [Pd(H)(X)(P^P)] (X = ligand),[31] or *via* reaction of a $Pd^{(II)}$-bis-sulfonate with methanol.[4a] Furthermore, palladium dihalides are known to react with acids to form Pd-hydride species [Pd(H)(X)(P^P)].[32] Since even palladium nanoparticles in the presence of Phanephos ligands and acids have been shown to promote methoxycarbonylation with similarly good *e.r.*,[33] it is reasonable to assume that various different pre-catalyst formulations can lead to an active catalyst of the type [Pd(H)(X)(P^P)]. Such species have been used in other computational studies on the mechanism of alkoxycarbonylation[4a] or hydroxycarbonylation[5] of other alkenes. In the reaction under study, the pre-catalyst is the dichloride complex $[PdCl_2(L)]$ (L = Phanephos ligand); initial computations (Figure S5) identified species $[Pd(H)(CO)(L)]^+$ (**1**) as the active catalyst, with similar structures with other ligands available for coordination (MeOH or Cl^-, as well as the substrate-bound complex **2**) being higher in energy, due to the strong back-bonding interaction afforded through the carbonyl ligand. The three-coordinate $\mathbf{[Pd(H)(L)]^+}$ species was found to be high in energy (ΔG_{RRS} = 15.9 kcal mol^{-1}).

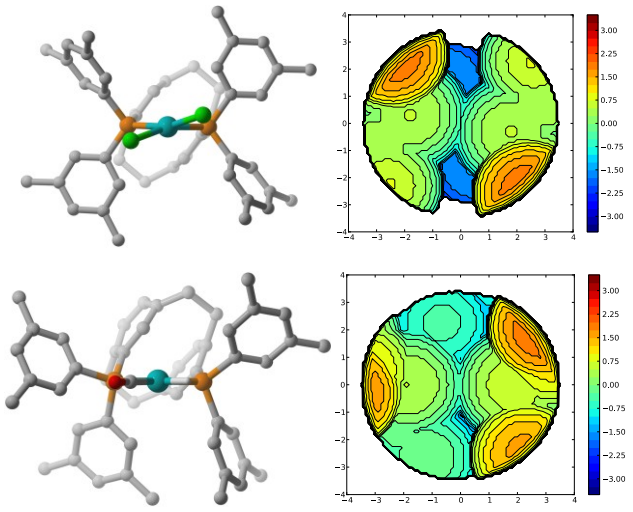

Figure 2. Optimized geometries and topographic steric maps of $[PdCl_2(L)]$ (top) and $[Pd(H)(CO)(L)]^+$ (bottom). L = Xylyl-Phanephos ligand. Positive (red) values of the isocontour lines refer to the down half-sphere where the ligand protrudes towards the substrate.

The results of our computational investigation of the reaction mechanism of the methoxycarbonylation of styrene catalyzed by Pd/(*S*)-Phanephos are summarized in Scheme 2, which depicts the full catalytic cycle. The first step is alkene coordination (**TS1–2**), which proceeds *via* an associative interchange mechanism where styrene displaces the CO molecule (see the SI for a discussion of the unfavorable dissociative mechanism). The transition states leading to the pro-branched and pro-linear species are shown in Figure 1. While $[PdCl_2(L)]$ has a symmetry axis (approximately C_2 symmetry), the presence of two different ligands (CO and H) in **1** breaks that symmetry, leading to four inequivalent quadrants (Figure 2 and Table S3). The structure of Phanephos (Figure 2) is interesting due to the rigidity of the paracyclophane backbone and its proximity to the pseudo-axial aryl rings on the phosphorous atoms, thus hindering free rotation around the P–aryl bond. The pseudo-axial rings are set face on to the paracyclophane CH_2 bridge, while the two remaining pseudo-equatorial rings are forced into an edge on orientation to minimize steric interactions with the pseudo-axial aryl rings. This is the structural orientation observed in all optimized intermediates and transition states. Despite this rigidity, there is a degree of freedom of rotation around the paracyclophane–P bond and, as such, the symmetry observed in $[PdCl_2(L)]$ can be broken (*e.g.*, $[Pd(H)(CO)(L)]^+$). This leads to three of the four quadrants shown in Figure 1 being effectively blocked. Species $[PdCl_2(L)]$ and $[Pd(H)(CO)(L)]^+$ can also be analyzed in terms of their topographic steric maps and buried volume (Figure 2 and Table S3).[30, 34] The percent buried volume (% V_{Buried}) describes differences in steric bulkiness of a ligand. $[PdCl_2(L)]$ was found to have a % V_{Buried} of 55.8: comparing this to other several well-known ligands, Phanephos is revealed to be bulkier than DPPE (46.8) and Xantphos (49.8), but less bulky than DTBPX (65.6). Performing the same buried volume analysis on intermediate **1** ($[Pd(H)(CO)(L)]^+$) results in a similar % V_{Buried} of 57.9, but with a significantly different steric map (Figure 2, bottom). While $[PdCl_2(L)]$ has a symmetry axis, **1** has broken that symmetry. The volume buried in each quadrant is quantified in Table S3: both "eastern" quadrants are bulkier than the "western" ones, with the "NW" quadrant the least sterically hindered one. Throughout the catalytic cycle, the preference for the smaller ligand to sit in the eastern quadrants is upheld.

To generate the pro-(*S*) and pro-L species, coordination of styrene to Pd occurs in the relatively unencumbered "north-western (NW)" quadrant (in the orientation in Figure 1); on the other hand, styrene has to approach **1** from the more sterically congested "south-western (SW)" quadrant to yield the pro-(*R*) Pd-olefin complex. This two-dimensional quadrant-diagram representation can partly rationalize the differences in free energies between the three isomeric TSs ($\Delta G_{RRS}^{\ddagger}$ = 12.3 kcal mol^{-1} (*S*), 16.2 (*R*) and 14.9 L). Distortion/interaction analysis (Figure S7) further helps to elucidate the origin of enantio- and regio-control in this selectivity-determining step. Although the substrate can be accommodated in the free "NW" quadrant, the geometry of **TS1–2-L** is significantly distorted with respect to the more stable (*S*)-counterpart. In **TS1–2-(*R*)**, not only the catalyst has to distort, but the substrate has to be placed in the more sterically congested "SW" quadrant. Another conformer of the linear TS, in which styrene sits in the sterically congested "SW" quadrant, has not been considered, since coordination of styrene in the sterically congested "SW" quadrant was already shown to increase the TS energy (as is the case of the (*R*)-TS). The pro-linear species generated from this transition state, **2-L conf2** (Figure 3), is however connected to the pro-(*S*) species *via* a different mechanism (*vide infra*).

Alkene coordination yields the Pd-olefin species **2-(*R*)/(*S*)** and **2-L**. Olefin insertion into the Pd–H bond (**TS2–3**) leads to the branched or linear Pd-alkyl species **3-(*R*)/(*S*)** and **3-L**, which involve sharing of the transferred hydride between carbon and palladium in an agostic bond. It is also during this step on the branched pathway that the stereochemistry of the ester product is set. The branched σ-complexes are in equilibrium with the energetically more stable π-complexes (Pd(II)-

η^3-benzyl species),[35] which can be regarded as off-cycle intermediates (see Figure S8 for further details). In intermediate **4**, the agostic bond is broken and replaced by another ligand. CO and Cl^- have both been examined as additional ligands, of which CO was found to be more energetically favorable (by *ca*. 1 kcal mol^{-1}, see Figure S10). CO coordination to the metal and subsequent insertion into the Pd–alkane bond (**TS4–5**) leads to the formation of acyl species **5-(*R*)/(*S*)** and **5-L**. In **TS4–5**, the smaller CO ligand preferably sits in the relatively more encumbered "eastern" coordination site; if the larger alkyl ligand occupies this quadrant, then the resulting structures (not shown) are all considerably higher in energy. Palladium-acyl species **5-L** and **5-(*R*)/(*S*)** again involve sharing the stereogenic CH between carbon and palladium in an agostic bond. Breaking this bond and adding an additional ligand lowers the energy considerably. Chloride, methanol and carbon monoxide complexes have been investigated. Methanol complexes are involved in the subsequent methanolysis step (*vide infra*), however CO and chloride are indicated to be much more strongly bound. In fact, the neutral chloride complexes **pro-(*R*)/(*S*)** and **pro-L** are computed to be more stable than other cationic complexes (by *ca*. 3 kcal mol^{-1}, see Figure S10). The preference for the chloride ligand in **pro-(*R*)/(*S*)** and **pro-L**, in contrast to the cationic carbonyl complexes **4**, can be rationalized by the acyl group in **5** being less electron-donation than the strongly donating alkyl group in **4**. Intermediates **pro-(*R*)/(*S*)** and **pro-L** were computed with inclusion of an explicit solvent molecule due to well-known shortcomings of the PCM model for bare Cl^-.[36,37] **Pro-(*R*)/(*S*)** and **pro-L** are included in Scheme 2 as they were found to be the lowest energy species in the cycle herein discussed. Even though they are effectively off-cycle intermediates, because the chloride ligand is assumed to dissociate to enable the subsequent methanolysis, they are important for the overall energy span of the whole cycle (*vide infra*). Methanolysis proceeds *via* outer-sphere attack of the nucleophile on the Pd-acyl complex (Pd–(C=O)R), rather than *via* reductive elimination of the ester from a Pd-methoxy-carbonyl species.[38] Although it is shown as a single step in Scheme 2, this process is actually a more complex sequence of steps, potentially involving more than one MeOH solvent molecule. Before discussing this step in more detail, we turn to the question of reversibility and isomerization, which is key for computing selectivities.

Reversibility as Revealed by Deuterium Labeling Studies. Two structurally similar catalysts giving such contrasting regioselectivity while retaining the same sense and level of stereoselectivity could involve the unselective catalyst (Pd/Xylyl-Phanephos) having a reversible branched ester cycle, while the electron-poor selective catalyst (Pd/F24-Phanephos) being essentially irreversible. To investigate if this was the case, *d*-labelling studies were carried out using d_4-MeOH and *d*-PTSA (PTSA = *p*-toluenesulfonic acid). While it is not possible to fully quantify subtle differences using ^{13}C and ^{2}H NMR, and a deutero-methoxycarbonylation is not a completely identical reaction to a hydro-methoxycarbonylation, it was envisaged that any clear-cut differences between the catalysts would be revealed. The key aspect to look at is the position of *d*-incorporation in the linear product: a straight hydro-methoxycarbonylation mechanism requires the *d*-label to end up on the carbon beta to the ester (**L** in Scheme 3); the formation of some linear ester (**L*** in Scheme 3) with the *d*-label on the carbon alpha to the ester is evidence that some of the linear product arises from the branched alkyl species, or, as has been subsequently established by DFT, from the branched acyl species **pro-(*S*)/(*R*)/L**. This can occur through the branched Pd-bound olefin species **2** *via* **TS2-(*S*)–2-L** (*vide infra*). ^{13}C NMR analysis (see the SI) clearly shows the presence of a deuterated carbon alpha to the ester functionality for the Pd/Xylyl-Phanephos catalyst, but only a trace of this is observed in the baseline for the Pd/F24-Phanephos catalyst. Scheme 3 shows the simpler ^{2}H NMR spectra: these agree fully with the ^{13}C NMR spectra, with the middle resonance assigned to **L*** being very different in magnitude for the two catalysts.

Scheme 3. Products of Deutero-Methoxycarbonylation of Styrene with Pd/(*R*)-Xylyl- and Pd/(*R*)-F24-Phanephos Catalysts as Revealed by ^{2}H NMR.

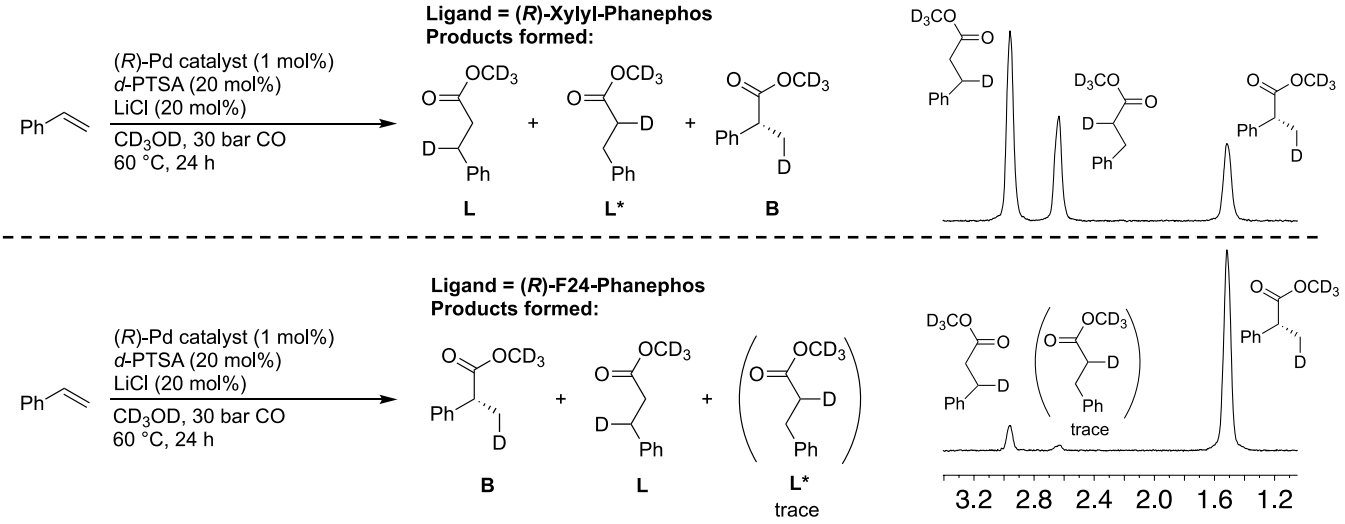

Based on this evidence, we can say with high confidence that the Pd/Xylyl-Phanephos–styrene catalytic cycle is significantly reversible, with much of the linear product arising from the branched ester cycle diverting onto the linear ester cycle. This phenomenon is barely seen with the regioselective F24-Phanephos-based catalyst, which generates very little **L***

product. There were no signs of other side products that could eliminate *d*-styrene, such as *d*-1-chloroethylbenzene, but if this did accompany the catalytic chemistry at a low level, it would do so to the same extent for both catalysts; the key finding *i.e.*, the unselective catalyst yielding a greater amount of deuteration on the carbon alpha to the linear ester, arises from differences between the catalysts themselves. Since these differences are quite stark, it is reasonable to assume similar differences between catalysts will have occurred in the non-deuterated experiments that were carried out in references 14a, 14b. The DFT computations are therefore expected to confirm the energies of later steps in the cycle as being higher or similar to the energies of the barriers for the branched ester diverting onto the linear ester pathway; on the other hand, the Pd/F24-Phanephos catalyst should be essentially irreversible.

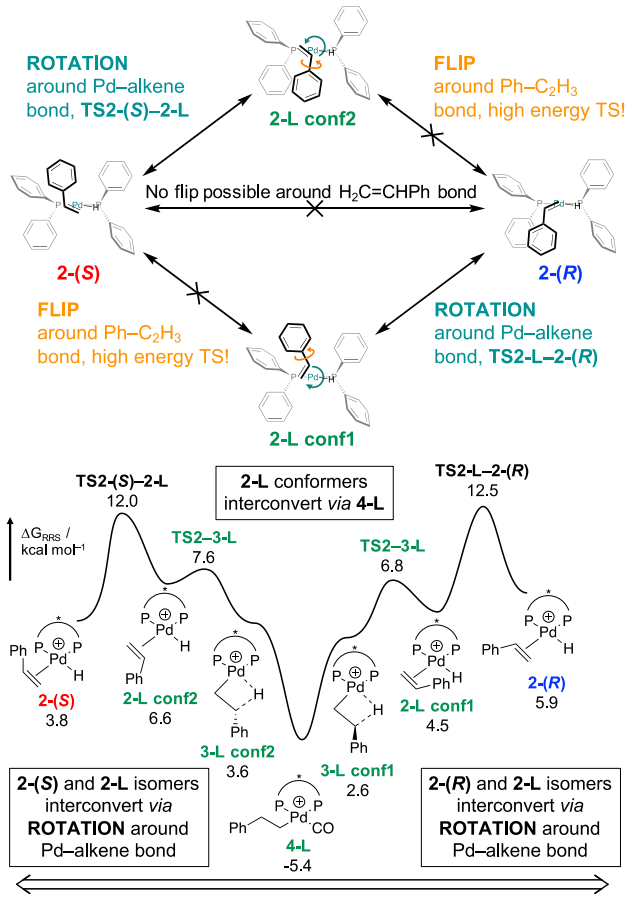

Figure 3. (Top) Scheme showing the isomerization mechanism for interconversion of Pd-bound olefin species. (Bottom) Potential energy surface of the isomerization mechanism with the Pd/(*S*)-Xylyl-Phanephos catalyst. B3PW91-D3-PCM$_{methanol}$/6-311+G(d,p)/SDD//B3PW91-D3/6-31G(d,p)/SDD, energies are Gibbs free energies, in kcal mol^{-1}, relative to **1**.

Isomerization Mechanism as Indicated by DFT Computations. Regioselectivity (B/L ratio) is determined at the stage of the palladium-olefin complexes **2**; additionally, the stereochemistry (*R*/*S* ratio) is set at the stage of the alkyl species **3-(*R*)/(*S*)** on the branched pathway. If all steps were irreversible, three separate catalytic cycles would ensue and the selectivities would be determined by the relative free energy spans of each of these cycles.[39,40] However, palladium-alkyl species **3-L** and **3-(*R*)/(*S*)** can convert back to the olefin-bound Pd-hydride intermediates *via* β-hydride elimination, the microscopic reverse of 1,2-insertion of olefins into metal-hydride bonds. It is well established that this step, when combined with olefin rotation and readdition, allows H migration to occur to either end of the olefin, a process related to that occurring during "chain running" or "chain walking" of the metal along the length of an alkyl chain during olefin polymerization.[41]

We highlight below a mechanism by which selectivity can be affected, namely by interconversion of pro-linear and pro-branched Pd-alkene species. This isomerization pathway is shown in Figure 3. A simple 180° rotation around the palladium–alkene bond converts intermediate **2-(*S*)** into the conformer of **2-L** with the styrene substrate in the relatively sterically congested "SW" quadrant (**2-L conf2**). To generate the more energetically stable **2-L conf1** (with styrene in the relatively unencumbered "NW" quadrant), the olefin would have to undergo a "flip" around the Ph–CHCH$_2$ bond, exchanging the face bound to the metal. This process is found to have a prohibitively high transition state ($\Delta G_{RRS}^{\ddagger}$ = 22.5 kcal mol^{-1}, not shown) and is therefore excluded from the mechanistic picture. Similarly, **2-(*R*)** can convert to conformer 1 of **2-L** *via* rotation around the Pd–(C=C) single bond, but would have to overcome a high-energy barrier to generate conformer 2 *via* a "flip" around its Ph–CHCH$_2$ bond. Direct interconversion of **2-(*S*)** and **2-(*R*)**, or of **2-L conf1** and **conf2**, would have to proceed via a "flip" around the H$_2$C=C(H)Ph bond, again exchanging the face of the alkene bound to the metal. This movement is sterically hindered by the pseudo-equatorial phenyl ring in the "NW" quadrant and therefore unlikely to occur. The two conformers of **2-L** are however connected in a different way along the reaction path: after olefin insertion into the Pd–H bond and addition of the CO ligand, the agostic bond in **3** is broken and free rotation possible around the Pd–C bond is possible, allowing structures **3-L conf1** and **2** to converge to one low energy minimum, **4-L**. In the reverse process, after CO dissociation from **4-L**, either of the hydrogen atoms at the β-position can participate in the agostic interaction with Pd, pushing the phenyl ring into either the "NW" or "SW" quadrant; β-hydride elimination then leads to conformer 1 or 2 of **2-L**. The pro-(*S*) and pro-(*R*) Pd-olefin bound species are therefore directly connected *via* the rotation transition states (their optimized geometries shown in Figure 2) and the pro-linear species. Compared to the unfavorable linear or (*R*)-branched alkene coordination transition states (**TS1–2**), this mechanism provides a lower energy pathway for the formation of the pro-(*R*) and pro-linear Pd-alkenes starting from **2-(*S*)**, which is effectively the sole species formed at **TS1–2** (96-98% selectivity).

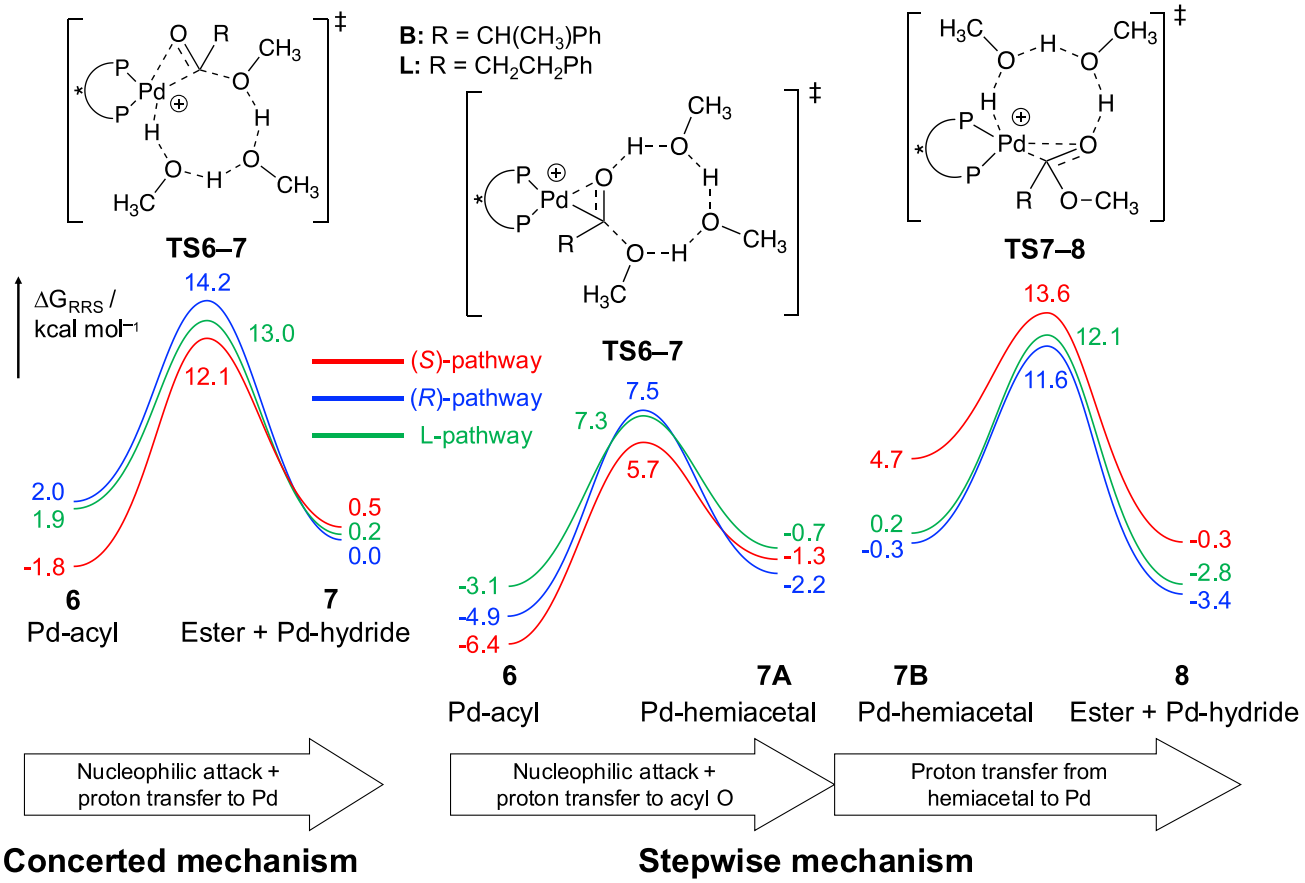

Figure 4. PES of methanolysis mechanisms with the Pd/(*S*)-Xylyl-Phanephos catalyst. B3PW91-D3-PCM$_{methanol}$/6-311+G(d,p)/SDD//B3PW91-D3/6-31G(d,p)/SDD, energies are Gibbs free energies, kcal mol^{-1}, relative to **1**. (Left) Concerted mechanism, showing the transition state for the simultaneous attack of methanol on the Pd-acyl carbon atom and proton transfer to Pd. (Right) Stepwise mechanism, showing on the left the transition state for nucleophilic attack of methanol and simultaneous proton transfer to the Pd-acyl oxygen atom, and on the right the transition state for proton transfer from the acyl oxygen to Pd.

Methanolysis. In the final step of the catalytic cycle, methanolysis, a solvent molecule attacks the Pd-acyl species **5**, yielding the corresponding linear or branched esters, which, initially coordinated to the metal, can be exchanged against a CO molecule, liberating the ester product and regenerating the Pd-hydride active catalyst **1** (see the SI for more details on this regeneration). With a single MeOH molecule attacking the acyl species, the concomitant transfer of the proton to Pd would have to proceed through energetically high-lying four-membered ring TSs. From initial studies with ethene as a model substrate, it transpired that additional MeOH molecules forming longer proton-relay chains successively reduce the total barrier (see Table S4). We have used up to three participating MeOH molecules. In the following, we will discuss the key results for the system with styrene as substrate and three methanol molecules, which was constructed from these initial computations.

The methanolysis step is difficult to model accurately due to the conformational variety in arranging the participating nucleophile and solvent molecules, and counterion(s) (if present).[5] It is further complicated by additional mechanistic alternatives: as shown in Figure 4, methanolysis can proceed in a concerted fashion when a proton is transferred directly from a methanol molecule to the palladium atom, with concomitant addition of a methoxide to the acyl carbon of the Pd-acyl complex. This has been described as an example of α-bond metathesis.[42] Alternatively, this step can proceed in a stepwise manner, if the proton is first transferred to the oxygen atom of the acyl-species as the new acetyl-carbon –methoxide bond is formed, generating a palladium-hemiacetal (Pd–C(OH)(OCH$_3$)R). Subsequently, to re-enter the catalytic cycle, the proton from the palladium-hemiacetal must be removed to form the ester product and transferred to palladium to re-generate the catalytically active Pd-hydride (**TS7–8**). **7A** and **7B** in Figure 4 are the end structures of the IRC computations of **TS6–7** and **TS7–8**, respectively, and differ in the relative orientation of the two methanol molecules that act as proton shuttle, while the third from the preceding step has been incorporated into the product. The optimized geometries of the kinetically relevant methanolysis transition states on the branched or linear pathways (*i.e.*, the highest on the pathways with overall lowest methanolysis barriers), either from the stepwise or concerted mechanism, are shown in Figure 5. These regio- and stereoisomeric TSs on the different pathways are rather similar in energy (an analysis of their relative stability is attempted in the SI). Evaluating the resulting overall selectivities is complicated by the aforementioned isomerization process. The final step of the catalytic cycle (methanolysis) occurs after the enantioselectivity is determined (at the stage of the alkyl species). Additionally, a regiochemical bias occurs in the earlier alkene insertion stage of the cycle. However, if methanolysis has a higher energy barrier from the

resting state (**pro-(*S*)**, selectively formed from **TS1–2**) than reverting back to the Pd-alkyl species (**3-(*S*)**), which is capable of isomerizing to the linear species (after β-hydride elimination and rotation around the Pd–olefin bond), methanolysis can cause the regiochemical bias from the alkene insertion step to be lost. This is the case of the unselective Pd/(*S*)-Xylyl-Phanephos catalyst, whereas with the selective Pd/(*S*)-F24-Phanephos catalyst the (*S*)-methanolysis process is enhanced relative to the isomerization pathway. These issues will be analyzed and discussed in more detail in the following section. We stress that, due to the interconnected nature of the three isomeric pathways, the energy span model cannot be used to compute the selectivity of the catalytic systems (by considering the difference between the energies of the methanolysis TSs and those of the resting state).

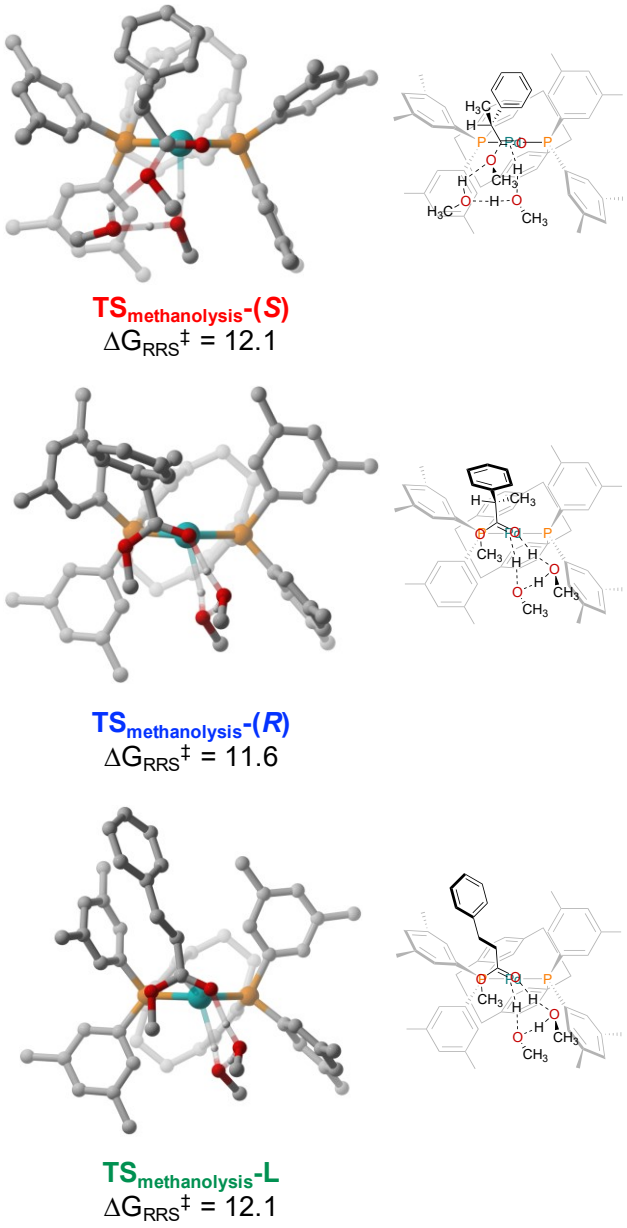

Figure 5. Optimized geometries and relative free energies of the kinetically significant transition states for methanolysis along the branched and linear pathways with the Pd/(*S*)-Xylyl-Phanephos catalyst. Energies are Gibbs free energies in kcal mol^{-1} relative to **1**.

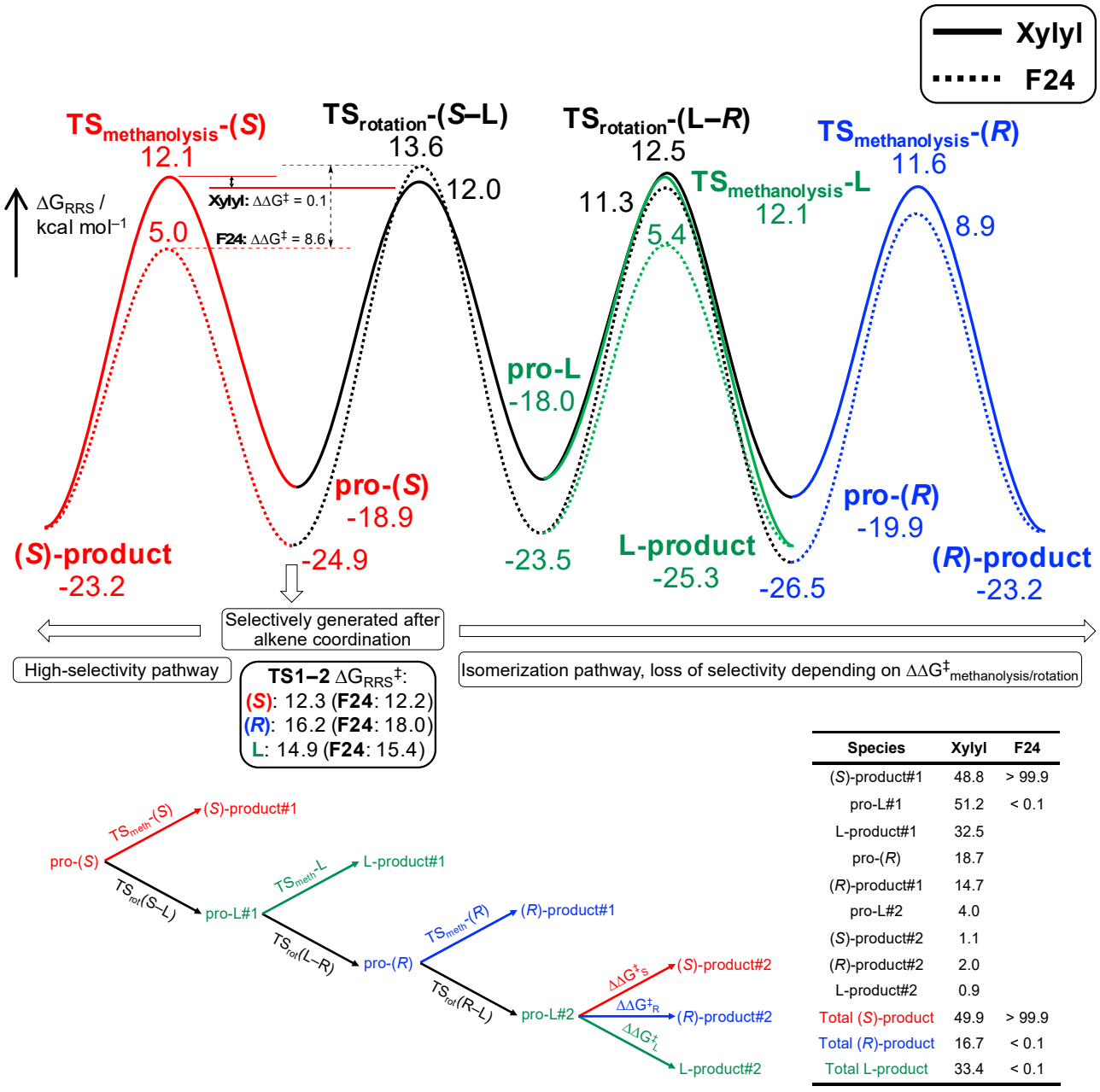

Species	Xylyl	F24
(*S*)-product#1	48.8	> 99.9
pro-L#1	51.2	< 0.1
L-product#1	32.5	
pro-(*R*)	18.7	
(*R*)-product#1	14.7	
pro-L#2	4.0	
(*S*)-product#2	1.1	
(*R*)-product#2	2.0	
L-product#2	0.9	
Total (*S*)-product	49.9	> 99.9
Total (*R*)-product	16.7	< 0.1
Total L-product	33.4	< 0.1

Figure 6. (Top) Simplified potential energy surface of the catalytic cycles of Pd/(*S*)-Xylyl- and Pd/(*S*)-F24-Phanephos showing competing methanolysis and rotation barriers. B3PW91-D3-PCM$_{methanol}$/6-311+G(d,p)/SDD//B3PW91-D3/6-31G(d,p)/SDD, energies are Gibbs free energies, in kcal mol^{-1}, relative to **1**. (Bottom) Branching workflow used to calculate selectivities (percentages in the table on the right), showing partitioning of the species according to the methanolysis and rotation TSs, and accounting for reversibility. ΔΔG‡$_{S/R/L}$ is the difference in free energy between the methanolysis TSs.

Kinetic Analysis of Methanolysis *vs.* Isomerization Pathways. As reported in Table S1, the barriers for the methanolysis step and those of the aforementioned isomerization mechanism for the Pd/(*S*)-Xylyl-Phanephos system are of a similar order of magnitude (in fact, this is a consequence of the necessary adjustment of the MHP correction to agree with the *d*-labelling results, see the SI). In this case, a particular regioisomer (B/L), before going to product *via* methanolysis, can revert back to the other regioisomer. This situation is illustrated by a simplified version of the potential energy surface (PES) of the full catalytic cycle, for both Pd/Xylyl- and Pd/F24-Phanephos, shown in Figure 6. Here, the Pd-acyl species **pro-(*R*)/(*S*)** and **pro-L** are included as the energy minima, connected by the rotation transition states **TS$_{rotation}$** (*i.e.*, **TS2-(*S*)–2-L** and **TS2-L–2-(*R*)** in Figure 3). **TS$_{methanolysis}$** are the kinetically relevant barriers that lead from the Pd-acyl intermediates to the branched or linear ester products (Figure 5). The starting point for the kinetic analysis of the PES is intermediate **pro-(*S*)**, which is generated from species **2-(*S*)** after alkene insertion into the Pd–H bond (**TS2–3**, ΔG$_{RRS}$‡ = 5.6 kcal mol^{-1}) and CO migratory insertion (**TS4–5**, ΔG$_{RRS}$‡ = -0.2 kcal mol^{-1}). Both of these steps are more favorable than rotation of the alkene around the Pd–(C=C) bond or methanolysis. Because **TS1–2** is highly selective, **pro-(*S*)** is assumed to be the only species generated after alkene coordination. From **pro-(*S*)**, the system can either undergo methanolysis and generate the (*S*)-ester, or revert back to the Pd-alkene species and isomerize to the linear Pd-acyl. The ratio of **pro-L** and **(*S*)-product** is given by eq. 1, where ΔΔG‡ is the difference between the (*S*)-methanolysis transition state and

$\mathbf{TS_{rotation}}$**-(S–L)**, R is the ideal gas constant (in kcal mol^{-1} K^{-1}) and T = 333.15 K.

$$\frac{(S)-\textbf{product}}{\textbf{pro-L}} = e^{\frac{-\Delta\Delta G^{\ddagger}}{RT}} \quad (1)$$

The fraction of **pro-(*S*)** converted to the pro-linear palladium-acyl can undergo methanolysis or isomerize *via* Pd–(C=C) bond rotation to yield **pro-(*R*)**. The ratio of **L-product** and **pro-(*R*)** is given by an expression similar to eq. 1, depending on the difference between $\mathbf{TS_{rotation}}$**-(L–R)** and $\mathbf{TS_{methanolysis}}$**-L**. To account for reversibility, the **pro-(*R*)** fraction thus generated is partitioned according to the (*R*)-methanolysis transition state and the (*R*)–L isomerization barrier into **(*R*)-product** and a further fraction of **pro-L**. The latter is then divided into the three isomeric ester products according to the relative differences between the methanolysis TSs ($\Delta\Delta G^{\ddagger}_{S/R/L}$). This is important in the limiting scenario where the barriers for interconversion between all isomers before methanolysis are fast and reversible (Curtin-Hammett-like scenario, see SI for further details). The branching workflow so far described is reported in Figure 6 (bottom), along with the percentages of each species generated from **pro-(*S*)**. This model allows us to calculate the final product distribution, which is 50% (*S*), 17% (*R*) and 33% L, for the Xylyl-Phanephos catalyst. This translates to a computed branched to linear ratio of 67:33 (2.0) and *e.r.* of 75:25 favoring (*S*). In the context of a subtle process such as this, where selectivity is determined by the competition of transition states from distinct parts of the cycle with different molecularities (5 molecules react together in $\mathbf{TS_{methanolysis}}$ *vs*. 2 in $\mathbf{TS_{rotation}}$) but similar energies, the agreement with the experimental results of 40:60 (0.7) and 90:10 *e.r.* is respectable (at 333.15 K, the difference between experimental and computed values translate to an error in $\Delta\Delta G^{\ddagger}$ of 0.7 kcal mol^{-1}).

Fluorinated Derivative. The validity of our computed mechanism is supported by the observed bias towards branched ester formation upon modification of the ligand electronic properties. The Pd/F24-Phanephos catalyst with electron-withdrawing $-CF_3$ groups (instead of $-CH_3$) is remarkably both regio- and stereoselective, much more so than its Pd/Xylyl-Phanephos parent. Key stationary points for the F24 system were re-optimized starting from the Pd/Xylyl-Phanephos minima and TSs (see SI for more details). In the Pd/F24-Phanephos system, the (*S*)-methanolysis TS (Figure 7 and dotted lines in Figure 6) lies 7.1 kcal mol^{-1} lower in energy than its Xylyl-counterpart. Pd-acyl species formed with the electron-withdrawing F24 ligand are more electron-deficient than their Xylyl-counterparts, and therefore more prone to nucleophilic addition of methanol, thus explaining the overall reduction in the methanolysis TS energies. Since the (*S*)–L rotation barrier is *not* equally reduced, this effectively makes the isomerization pathway energetically prohibitive and unable to compete with **(*S*)-product** formation. The high branched selectivity observed with the electron-deficient catalyst is therefore reproduced by our computations, thus lending further support to the mechanistic scenario that we have outlined. We emphasize that, although Figure 7 provides a comprehensive picture of the stationary points on the Pd/(*S*)-F24-Phanephos PES, the three isomeric pathways should *not* be regarded as independent, and selectivity be computed from the respective energy spans. This is because the pathways are connected by the rotation transition states (Figure 3, top, and Figure S9) and thus have a common intermediate (species **pro-(*S*)**, selectively generated after alkene coordination, **TS1–2**). Regio- and enantioselectivity are therefore calculated using the branching workflow and the simplified PES shown in Figure 6.

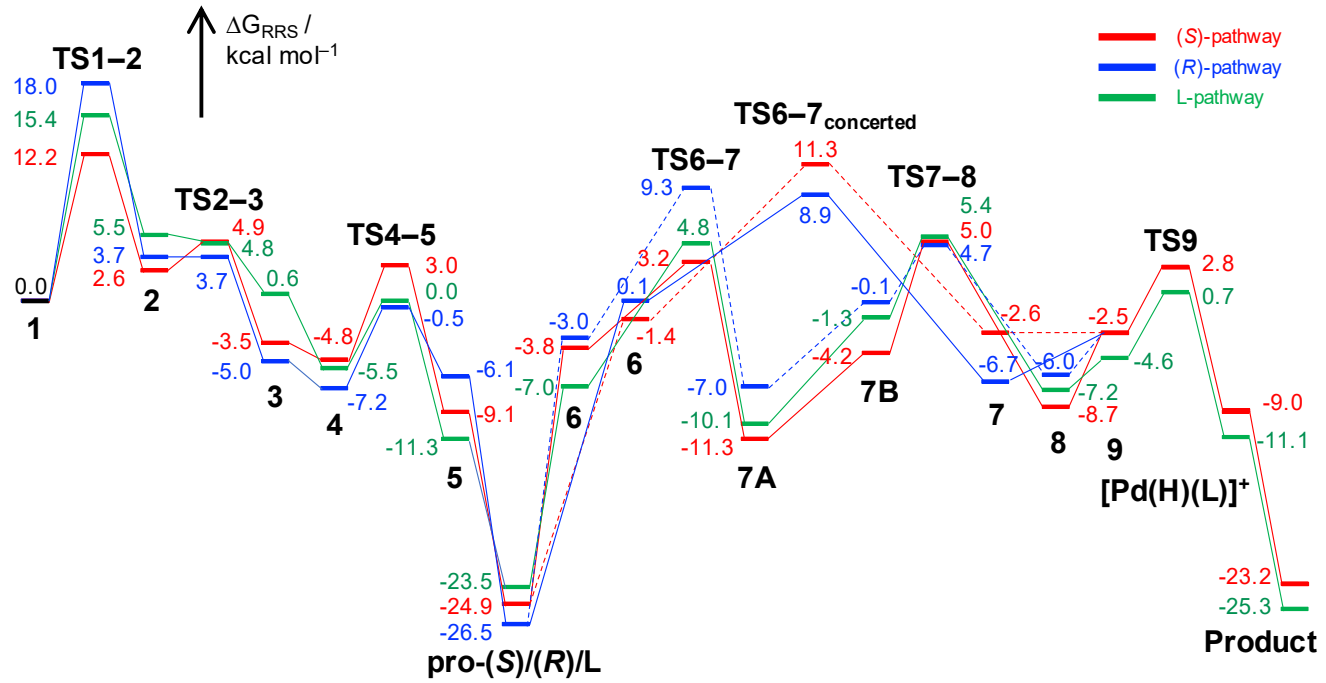

Figure 7. Potential Energy Surface for the methoxycarbonylation of styrene with the selective Pd/(*S*)-F24-Phanephos catalyst. B3PW91-D3-$PCM_{methanol}$/6-311+G(d,p)/SDD//B3PW91-D3/6-31G(d,p)/SDD, energies are Gibbs free energies, in kcal mol^{-1}, relative to **1**.

CONCLUSIONS

In summary, on the basis of DFT computations supported by deuterium labeling studies, we have investigated the detailed reaction mechanism of the methoxycarbonylation of styrene with Pd/Phanephos catalysts (Scheme 2) to gain better understanding of the origin of the ligand electronic effect that leads to high branched regioselectivity. The low symmetry in the Pd-Phanephos active catalyst makes the quadrants of the catalytic pocket inequivalent: alkene coordination is highly selective for the pro-(*S*) Pd-bound olefin complex, in both the parent and fluorinated catalysts. We have shown how pro-branched and pro-linear Pd-alkene complexes can isomerize *via* rotation around the metal–(C=C) bond. This process leads to loss of selectivity when its energy barrier is similar to that *via* the methanolysis transition state, as is the case with the Xylyl-Phanephos ligand. Indeed, this catalyst shows poor branched regioselectivity. Furthermore, our mechanism is consistent with the observation that reduced levels of electron density on palladium are instrumental for the control of regioselectivity. With a highly electron-withdrawing ligand (F24-Phanephos), the (*S*)-methanolysis process is enhanced relative to the isomerization pathway, allowing the pro-(*S*) species to directly undergo methanolysis and enabling essentially perfect branched regioselectivity.

The interesting ligand effect in the Pd/Phanephos system is now understood with a useful level of detail. Branched selective carbonylation requires steric hindrance in specific zones of the catalytic pocket by a chiral bidentate ligand to prevent the formation of the linear Pd-acyl or of the other branched enantiomer. Monophosphines are unable to enforce a rigid enough coordination sphere around the metal to lead to complete asymmetric induction. While unfavorable steric interactions between the branched alkyl species and the ligand have generally been proposed as the cause of poor regioselectivity in bidentate ligand systems, these do not seem to play a significant role in Pd/Phanephos catalysts (with the branched Pd-alkyl species being 8.0 kcal mol^{-1} lower in energy than the Pd-hydridocarbonyl species **1**). Ligand electronic effects that lower the methanolysis barrier with respect to the reverse reaction and prevent isomerization from the branched to the linear alkyl species are key to obtaining high regioselectivity in the current system. The computations show that the less donating Phanephos ligand significantly lowers the activation energy of the methanolysis step in the catalytic cycle ($\Delta G^{\ddagger}_{F24}$ = 9.2 kcal mol^{-1} *vs*. $\Delta G^{\ddagger}_{Xylyl}$ = 13.9 kcal mol^{-1}). This significant difference therefore quite likely explains the high branched regioselectivity observed using catalysts derived from other less electron-donating diphosphine ligands,[11, 13a, 16] or suggests that faster methanolysis using less strongly donating ligands occurs.[43] The design of improved catalysts that require more efficient methanolysis processes in their catalytic cycles should consider using this fluorine-related effect within the ligand to achieve this.

ASSOCIATED CONTENT

Supporting Information

The Supporting Information is available free of charge on the ACS Publications website.

Computational details, ^{2}H and ^{13}C NMR spectra, deuterium labeling studies (PDF)

Cartesian coordinates, electronic energies, zero-point energies, enthalpies, T×S, Gibbs free energies, basis set superposition energies (a.u.), imaginary frequencies (XYZ)

AUTHOR INFORMATION

Corresponding Authors

*mb105@st-andrews.ac.uk
*mc28@st-andrews.ac.uk

Present Address

‡Laboratory for Computational Molecular Design, Institute of Chemical Sciences and Engineering, Ecole Polytechnique Fedérale dé Lausanne (EPFL), 1015 Lausanne, Switzerland.

ACKNOWLEDGMENT

MB thanks the School of Chemistry and EaStCHEM for support. Calculations were performed on local computer clusters maintained by Dr H. Früchtl. Dr Bowen Xie (MChem University of St Andrews, 2014), and Dr Jamie Durrani (PhD University of St Andrews, 2014) are thanked for initial *d*-labelling studies. The EPSRC are thanked for funding PD and JAF in the very early stages of this work (EP/M003868/1).

REFERENCES

(1) (a) Leeuwen, P. W. N. M. V. *Homogeneous Catalysis: Understanding the Art*; Kluwer Academic Publishers: Dordrecht, 2004; (b) Gehrtz, P. H.; Hirschbeck, V.; Ciszek, B.; Fleischer, I., Carbonylations of Alkenes in the Total Synthesis of Natural Compounds. *Synthesis* **2016,** *48*, 1573-1596; (c) Bai, Y.; Davis, D. C.; Dai, M., Natural Product Synthesis via Palladium-Catalyzed Carbonylation. *J. Org. Chem.* **2017,** *82*, 2319-2328.

(2) (a) Clegg, W.; Eastham, G. R.; Elsegood, M. R. J.; Tooze, R. P.; Wang, X. L.; Whiston, K., Highly Active and Selective Catalysts for the Production of Methyl Propanoate *via* the Methoxycarbonylation of Ethene. *Chem. Commun.* **1999,** *0*, 1877-1878; (b) Eastham, G. R.; Heaton, B. T.; Iggo, J. A.; Tooze, R. P.; Whyman, R.; Zacchini, S., Synthesis and Spectroscopic Characterisation of All the Intermediates in the Pd-Catalysed Methoxycarbonylation of Ethene. *Chem. Commun.* **2000**, 609-610.

(3) (a) Pugh, R. I.; Drent, E.; Pringle, P. G., Tandem Isomerisation–Carbonylation Catalysis: Highly Active Palladium(II) Catalysts for the Selective Methoxycarbonylation of Internal Alkenes to Linear Esters. *Chem. Commun.* **2001**, 1476-1477; (b) Fanjul, T.; Eastham, G.; Fey, N.; Hamilton, A.; Orpen, A. G.; Pringle, P. G.; Waugh, M., Palladium Complexes of the Heterodiphosphine *o*-$C_6H_4(CH_2P^tBu_2)(CH_2PPh_2)$ Are Highly Selective and Robust Catalysts for the Hydromethoxycarbonylation of Ethene. *Organometallics* **2010,** *29*, 2292-2305; (c) Fanjul, T.; Eastham, G.; Haddow, M. F.; Hamilton, A.; Pringle, P. G.; Orpen, A. G.; Turner, T. P. W.; Waugh, M., Efficient and Chemoselective Ethene Hydromethoxycarbonylation Catalysts Based on Pd-complexes of Heterodiphosphines *o*-$C_6H_4(CH_2P^tBu_2)(CH_2PR_2)$. *Catal. Sci. Technol.* **2012,** *2*, 937-950; (d) Li, H.; Dong, K.; Jiao, H.; Neumann, H.; Jackstell, R.; Beller, M., The Scope and Mechanism of Palladium-Catalysed Markovnikov Alkoxycarbonylation of Alkenes. *Nat. Chem.* **2016,** *8*, 1159-1166; (e) Dong, K.; Fang, X.; Gülak, S.; Franke, R.; Spannenberg, A.; Neumann, H.; Jackstell, R.; Beller, M., Highly Active and Efficient Catalysts for Alkoxycarbonylation of Alkenes. *Nat. Commun.* **2017,** *8*, 14117; (f) Donald, S. M. A.; Macgregor, S. A.; Settels, V.; Cole-Hamilton, D. J.; Eastham, G. R., A computational study of the methanolysis of palladium–acyl bonds. *Chem. Commun.* **2007**, 562-564; (g) Zuidema, E.; Bo, C.; van Leeuwen, P. W. N. M., Ester versus Polyketone Formation in the Palladium−Diphosphine Catalyzed Carbonylation of Ethene. *J. Am. Chem. Soc.* **2007,** *129*, 3989-4000.

(4) (a) Roesle, P.; Durr, C. J.; Moller, H. M.; Cavallo, L.; Caporaso, L.; Mecking, S., Mechanistic Features of Isomerizing Alkoxycarbonylation of Methyl Oleate. *J. Am. Chem. Soc.* **2012,** *134*, 17696-703; (b) Furst, M. R. L.; Goff, R. L.; Quinzler, D.; Mecking, S.; Botting, C. H.; Cole-Hamilton, D. J., Polymer Precursors From Catalytic Reactions of Natural Oils. *Green Chem.* **2012,** *14*, 472-477; (c) Roesle, P.; Caporaso, L.; Schnitte, M.; Goldbach, V.; Cavallo, L.; Mecking, S., A Comprehensive Mechanistic Picture of the Isomerizing Alkoxycarbonylation of Plant Oils. *J. Am. Chem. Soc.* **2014,** *136*, 16871-81.

(5) Zhao, L.; Pudasaini, B.; Genest, A.; Nobbs, J. D.; Low, C. H.; Stubbs, L. P.; van Meurs, M.; Rösch, N., Palladium-Catalyzed Hydroxycarbonylation of Pentenoic Acids. Computational and Experimental Studies on the Catalytic Selectivity. *ACS Catal.* **2017,** *7*, 7070-7080.
(6) (a) Drent, E.; Ernst, R.; Jager, W. W.; Krom, C. A.; Nisbet, T. M. Process for the Carbonylation of a Conjugated Diene to a Dicarboxylic Acid. US20080269520, 2008; (b) Kathe, P.; Fleischer, I., Cooperative Use of Brønsted Acids and Metal Catalysts in Tandem Isomerization Reactions of Olefins. *ChemCatChem* **2019,** *11*, 3343-3354; (c) Low, C. H.; Nobbs, J. D.; van Meurs, M.; Stubbs, L. P.; Drent, E.; Aitipamula, S.; Pung, M. H. L., Palladium Complexes with Bulky Diphosphine Ligands as Highly Selective Catalysts for the Synthesis of (Bio-)Adipic Acid from Pentenoic Acid Mixtures. *Organometallics* **2015,** *34*, 4281-4292; (d) Goldbach, V.; Falivene, L.; Caporaso, L.; Cavallo, L.; Mecking, S., Single-Step Access to Long-Chain α,ω-Dicarboxylic Acids by Isomerizing Hydroxycarbonylation of Unsaturated Fatty Acids. *ACS Catal.* **2016,** *6*, 8229-8238.
(7) (a) Seayad, A.; Jayasree, S.; Damodaran, K.; Toniolo, L.; Chaudhari, R. V., On the Mechanism of Hydroesterification of Styrene Using an In Situ-Formed Cationic Palladium Complex. *J. Organomet. Chem.* **2000,** *601*, 100-107; (b) Benedek, C.; Szalontai, G.; Gömöry, Á.; Törös, S.; Heil, B., A Study on the Catalytic Pathways of the Hydroalkoxycarbonylation Reaction of Styrene. *J. Organomet. Chem.* **1999,** *579*, 147-155; (c) Eastham, G. R.; Tooze, R. P.; Kilner, M.; Foster, D. F.; Cole-Hamilton, D. J., Deuterium Labelling Evidence for a Hydride Mechanism in the Formation of Methyl Propanoate From Carbon Monoxide, Ethene and Methanol Catalysed by a Palladium Complex. *J. Chem. Soc., Dalton Trans.* **2002**, 1613-1617; (d) Kawana, M.; Nakamura, S.; Watanabe, E.; Urata, H., Hydroesterification of Ethylene Catalyzed by Pd(II) Complexes: An Ab Initio MO Study. *J. Organomet. Chem.* **1997,** *542*, 185-189.
(8) Brennführer, A.; Neumann, H.; Beller, M., Palladium-Catalyzed Carbonylation Reactions of Alkenes and Alkynes. *ChemCatChem* **2009,** *1*, 28-41.
(9) Hendricks, J. D.; Mott, G. N. Method for Producing Ibuprofen. US5166418, 1992.
(10) Zapf, A.; Beller, M., Fine Chemical Synthesis with Homogeneous Palladium Catalysts: Examples, Status and Trends. *Top. Catal.* **2002,** *19*, 101-109.
(11) Frew, J. J.; Damian, K.; Van Rensburg, H.; Slawin, A. M.; Tooze, R. P.; Clarke, M. L., Palladium(II) Complexes of New Bulky Bidentate Phosphanes: Active and Highly Regioselective Catalysts for the Hydroxycarbonylation of Styrene. *Chem. - Eur. J.* **2009,** *15*, 10504-13.
(12) Harkness, G. J.; Clarke, M. L., A Highly Enantioselective Alkene Methoxycarbonylation Enables a Concise Synthesis of (*S*)-Flurbiprofen. *Eur. J. Org. Chem.* **2017,** *2017*, 4859-4863.
(13) (a) Guiu, E.; Caporali, M.; Munoz, B.; Muller, C.; Lutz, M.; Spek, A. L.; Claver, C.; van Leeuwen, P. W. N. M., Electronic Effect of Diphosphines on the Regioselectivity of the Palladium-Catalyzed Hydroesterification of Styrene. *Organometallics* **2006,** *25*, 3102-3104; (b) Ooka, H.; Inoue, T.; Itsuno, S.; Tanaka, M., Highly Active and Selective Palladium Catalyst For Hydroesterification of Styrene and Vinyl Acetate Promoted by Polymeric Sulfonic Acids. *Chem. Commun.* **2005**, 1173-1175; (c) del Rio, I.; Ruiz, N.; Claver, C.; van der Veen, L. A.; Leeuwen, P. W. N. M. V., Hydroxycarbonylation of Styrene with Palladium Catalysts: The Influence of the Mono- and Bidentate Phosphorus Ligand. *J. Mol. Catal. A: Chem.* **2000,** *161*, 39-48; (d) Miquel-Serrano, M. D.; Aghmiz, A.; Diéguez, M.; Masdeu-Bultó, A. M.; Claver, C.; Sinou, D., Recoverable Chiral Palladium–Sulfonated Diphosphine Catalysts for the Asymmetric Hydrocarboxylation of Vinyl Arenes. *Tetrahedron: Asymmetry* **1999,** *10*, 4463-4467; (e) Godard, C.; Ruiz, A.; Claver, C., Systematic Study of the Asymmetric Methoxycarbonylation of Styrene Catalyzed by Palladium Systems Containing Chiral Ferrocenyl Diphosphine Ligands. *Helv. Chim. Acta* **2006,** *89*, 1610-1622; (f) Oi, S.; Nomura, M.; Aiko, T.; Inoue, Y., Regioselective Hydroesterification of Styrene Catalyzed by Cationic Palladium(II) Complexes Under Mild Conditions. *J. Mol. Catal. A: Chem.* **1997,** *115*, 289-295.
(14) (a) Konrad, T. M.; Fuentes, J. A.; Slawin, A. M.; Clarke, M. L., Highly Enantioselective Hydroxycarbonylation and Alkoxycarbonylation of Alkenes Using Dipalladium Complexes as Precatalysts. *Angew. Chem. Int. Ed. Engl.* **2010,** *49*, 9197-200; (b) Konrad, T. M.; Durrani, J. T.; Cobley, C. J.; Clarke, M. L., Simultaneous Control of Regioselectivity and Enantioselectivity in the Hydroxycarbonylation and Methoxycarbonylation of Vinyl Arenes. *Chem. Commun.* **2013,** *49*, 3306-8; (c) Fuentes, J. A.; Durrani, J. T.; Leckie, S. M.; Crawford, L.; Bühl, M.; Clarke, M. L., Isomerisation *Versus* Carbonylative Pathways in the Hydroxy-Carbonylation, Methoxy-Carbonylation, and Amino-Carbonylation of *N*-tosyl-3-pyrroline. *Catal. Sci. Technol.* **2016,** *6*, 7477-7485.
(15) Adrio, L. A.; Hii, K. K. PhanePhos and Related Derivatives. In *Encyclopedia of Reagents for Organic Synthesis*; John Wiley & Sons, Ltd: 2012.
(16) Frew, J. J.; Clarke, M. L.; Mayer, U.; Van Rensburg, H.; Tooze, R. P., Palladium Complexes of New Bulky Fluorinated Diphosphines Give Particularly Active and Regioselective Catalysts for Hydroxycarbonylation of Styrene. *Dalton Trans.* **2008**, 1976-8.
(17) Li, J.; Chang, W.; Ren, W.; Dai, J.; Shi, Y., Palladium-Catalyzed Highly Regio- and Enantioselective Hydroesterification of Aryl Olefins with Phenyl Formate. *Org. Lett.* **2016,** *18*, 5456-5459.
(18) Frisch, M. J.; Trucks, G. W.; Schlegel, H. B.; Scuseria, G. E.; Robb, M. A.; Cheeseman, J. R.; Scalmani, G.; Barone, V.; Petersson, G. A.; Nakatsuji, H.; Li, X.; Caricato, M.; Marenich, A. V.; Bloino, J.; Janesko, B. G.; Gomperts, R.; Mennucci, B.; Hratchian, H. P.; Ortiz, J. V.; Izmaylov, A. F.; Sonnenberg, J. L.; Williams; Ding, F.; Lipparini, F.; Egidi, F.; Goings, J.; Peng, B.; Petrone, A.; Henderson, T.; Ranasinghe, D.; Zakrzewski, V. G.; Gao, J.; Rega, N.; Zheng, G.; Liang, W.; Hada, M.; Ehara, M.; Toyota, K.; Fukuda, R.; Hasegawa, J.; Ishida, M.; Nakajima, T.; Honda, Y.; Kitao, O.; Nakai, H.; Vreven, T.; Throssell, K.; Montgomery Jr., J. A.; Peralta, J. E.; Ogliaro, F.; Bearpark, M. J.; Heyd, J. J.; Brothers, E. N.; Kudin, K. N.; Staroverov, V. N.; Keith, T. A.; Kobayashi, R.; Normand, J.; Raghavachari, K.; Rendell, A. P.; Burant, J. C.; Iyengar, S. S.; Tomasi, J.; Cossi, M.; Millam, J. M.; Klene, M.; Adamo, C.; Cammi, R.; Ochterski, J. W.; Martin, R. L.; Morokuma, K.; Farkas, O.; Foresman, J. B.; Fox, D. J. *Gaussian 09*, Revision D.01;Gaussian, Inc.: Wallingford, CT, 2013.
(19) (a) Becke, A. D., Density-Functional Thermochemistry. IV. A New Dynamical Correlation Functional and Implications for Exact-Exchange Mixing. *J. Chem. Phys.* **1996,** *104*, 1040-1046; (b) Perdew, J. P.; Chevary, J. A.; Vosko, S. H.; Jackson, K. A.; Pederson, M. R.; Singh, D. J.; Fiolhais, C., Atoms, Molecules, Solids, and Surfaces: Applications of the Generalized Gradient Approximation for Exchange and Correlation. *Phys. Rev. B* **1992,** *46*, 6671-6687; (c) Perdew, J. P.; Burke, K.; Wang, Y., Generalized Gradient Approximation for the Exchange-Correlation Hole of a Many-Electron System. *Phys. Rev. B* **1996,** *54*, 16533-16539.
(20) Waller, M. P.; Braun, H.; Hojdis, N.; Bühl, M., Geometries of Second-Row Transition-Metal Complexes from Density Functional Theory. *J. Chem. Theory Comput.* **2007,** *3*, 2234-2242.
(21) Dolg, M.; Wedig, U.; Stoll, H.; Preuss, H., Energy-Adjusted Ab Initio Pseudopotentials for the First Row Transition Elements. *J. Chem. Phys.* **1987,** *86*, 866-872.
(22) Grimme, S.; Antony, J.; Ehrlich, S.; Krieg, H., A Consistent and Accurate Ab Initio Parametrization of Density Functional Dispersion Correction (DFT-D) for the 94 Elements H-Pu. *J. Chem. Phys.* **2010,** *132*, 154104.
(23) Dingwall, P.; Fuentes, J. A.; Crawford, L.; Slawin, A. M. Z.; Bühl, M.; Clarke, M. L., Understanding a Hydroformylation Catalyst that Produces Branched Aldehydes from Alkyl Alkenes. *J. Am. Chem. Soc.* **2017,** *139*, 15921-15932.
(24) (a) Tomasi, J.; Cammi, R.; Mennucci, B.; Cappelli, C.; Corni, S., Molecular Properties in Solution Described with a Continuum Solvation Model. *Phys. Chem. Chem. Phys.* **2002,** *4*, 5697-5712; (b) Tomasi, J.; Mennucci, B.; Cancès, E., The IEF Version of the PCM Solvation Method: An Overview of a New Method Addressed to Study Molecular Solutes at the QM Ab Initio Level. *J. Mol. Struct.: THEOCHEM* **1999,** *464*, 211-226.
(25) Boys, S. F.; Bernardi, F., The Calculation of Small Molecular Interactions by the Differences of Separate Total Energies. Some Procedures With Reduced Errors. *Mol. Phys.* **1970,** *19*, 553-566.
(26) Luchini, G.; Alegre-Requena, J. V.; Funes-Ardoiz, I.; Paton, R. S., GoodVibes: Automated Thermochemistry for Heterogeneous Computational Chemistry Data. *F1000Research* **2020,** *9*, 291.
(27) Martin, R. L.; Hay, P. J.; Pratt, L. R., Hydrolysis of Ferric Ion in Water and Conformational Equilibrium. *J. Phys. Chem. A* **1998,** *102*, 3565-3573.
(28) Fukui, K., The Path of Chemical Reactions - The IRC Approach. *Acc. Chem. Res.* **1981,** *14*, 363-368.
(29) Legault, C. Y. *CYLview, 1.0b*, Université de Sherbrooke, 2009; http://www.cylview.org.
(30) Falivene, L.; Cao, Z.; Petta, A.; Serra, L.; Poater, A.; Oliva, R.; Scarano, V.; Cavallo, L., Towards the Online Computer-Aided Design of Catalytic Pockets. *Nat. Chem.* **2019,** *11*, 872-879.

(31) Clegg, W.; Eastham, G. R.; Elsegood, M. R. J.; Heaton, B. T.; Iggo, J. A.; Tooze, R. P.; Whyman, R.; Zacchini, S., Characterization and Dynamics of $[Pd(L-L)H(solv)]^+$, $[Pd(L-L)(CH_2CH_3)]^+$, and $[Pd(L-L)(C(O)Et)(THF)]^+$ (L−L = 1,2-$(CH_2PBu^t_2)_2C_6H_4$): Key Intermediates in the Catalytic Methoxycarbonylation of Ethene to Methylpropanoate. *Organometallics* **2002,** *21*, 1832-1840.
(32) Blanco, C.; Godard, C.; Zangrando, E.; Ruiz, A.; Claver, C., Room Temperature Asymmetric Pd-Catalyzed Methoxycarbonylation of Norbornene: Highly Selective Catalysis and HP-NMR Studies. *Dalton Trans.* **2012,** *41*, 6980-6991.
(33) Konrad, T. M. Chiral Phanephos Derived Catalysts and Their Application in Asymmetric Catalysis. Ph.D. Thesis, University of St Andrews, UK, 2013. DOI: 10.17630/10023-4499.
(34) (a) Falivene, L.; Credendino, R.; Poater, A.; Petta, A.; Serra, L.; Oliva, R.; Scarano, V.; Cavallo, L., SambVca 2. A Web Tool for Analyzing Catalytic Pockets with Topographic Steric Maps. *Organometallics* **2016,** *35*, 2286-2293; (b) Poater, A.; Ragone, F.; Giudice, S.; Costabile, C.; Dorta, R.; Nolan, S. P.; Cavallo, L., Thermodynamics of N-Heterocyclic Carbene Dimerization: The Balance of Sterics and Electronics. *Organometallics* **2008,** *27*, 2679-2681; (c) Poater, A.; Ragone, F.; Mariz, R.; Dorta, R.; Cavallo, L., Comparing the Enantioselective Power of Steric and Electrostatic Effects in Transition-Metal-Catalyzed Asymmetric Synthesis. *Chem. - Eur. J.* **2010,** *16*, 14348-14353.
(35) Gatti, G.; López, J. A.; Mealli, C.; Musco, A., Structural and NMR Spectroscopic Characterization of η^3-Benzyl palladium(II) Complexes. *J. Organomet. Chem.* **1994,** *483*, 77-89.
(36) (a) da Silva, E. F.; Svendsen, H. F.; Merz, K. M., Explicitly Representing the Solvation Shell in Continuum Solvent Calculations. *J. Chem. Phys. A* **2009,** *113*, 6404-6409; (b) Tomasi, J.; Mennucci, B.; Cammi, R., Quantum Mechanical Continuum Solvation Models. *Chem. Rev.* **2005,** *105*, 2999-3094; (c) Skyner, R. E.; McDonagh, J. L.; Groom, C. R.; van Mourik, T.; Mitchell, J. B. O., A Review of Methods for the Calculation of Solution Free Energies and the Modelling of Systems in Solution. *Phys. Chem. Chem. Phys.* **2015,** *17*, 6174-6191; (d) Guerard, J. J.; Arey, J. S., Critical Evaluation of Implicit Solvent Models for Predicting Aqueous Oxidation Potentials of Neutral Organic Compounds. *J. Chem. Theory Comput.* **2013,** *9*, 5046-5058.
(37) The complexes are neutral, the reaction for their formation *e.g.*, $\mathbf{5}^{(+)} + Cl^{(-)} \rightarrow \mathbf{5\text{-}Cl}^{(0)}$, thus involves charge combination. Modelling solvation of a free chloride ion, which has a very high charge density, is a challenge for simple continuum models. Inclusion of one MeOH molecule alleviates this problem (also because an explicit solute-solvent interaction is now included) and raises the energy of the chloride intermediate by *ca*. 3 kcal mol^{-1}.
(38) (a) Grigg, R.; Mutton, S. P., Pd-catalysed Carbonylations: Versatile Technology for Discovery and Process Chemists. *Tetrahedron* **2010,** *66*, 5515-5548; (b) Schoenberg, A.; Bartoletti, I.; Heck, R. F., Palladium-Catalyzed Carboalkoxylation of Aryl, Benzyl, and Vinylic Halides. *J. Org. Chem.* **1974,** *39*, 3318-3326.
(39) (a) Kozuch, S.; Shaik, S., How to Conceptualize Catalytic Cycles? The Energetic Span Model. *Acc. Chem. Res.* **2011,** *44*, 101-110; (b) Kozuch, S.; Martin, J. M. L., What Makes for a Bad Catalytic Cycle? A Theoretical Study on the Suzuki−Miyaura Reaction within the Energetic Span Model. *ACS Catal.* **2011,** *1*, 246-253.
(40) As discussed in the kinetic analysis of the PES, applying the energy span model to this system is complicated by the interlocked nature of the three isomeric pathways. Because these can have common intermediates depending on the relative energies of the isomerization and methanolysis TSs, we take a different approach to calculate selectivities (see Figure 6).
(41) Rix, F. C.; Brookhart, M.; White, P. S., Electronic Effects on the β-Alkyl Migratory Insertion Reaction of *para*-Substituted Styrene Methyl Palladium Complexes. *J. Am. Chem. Soc.* **1996,** *118*, 2436-2448.
(42) del Río, I.; Claver, C.; Leeuwen, Piet W. N. M. V., On the Mechanism of the Hydroxycarbonylation of Styrene with Palladium Systems. *Eur. J. Inorg. Chem.* **2001,** *2001*, 2719-2738.
(43) Nobbs, J. D.; Low, C. H.; Stubbs, L. P.; Wang, C.; Drent, E.; van Meurs, M., Isomerizing Methoxycarbonylation of Alkenes to Esters Using a Bis(phosphorinone)xylene Palladium Catalyst. *Organometallics* **2017,** *36*, 391-398.